A workflow to evaluate the potential of the Emscher Formation as hydraulic barrier during mine water rebound in the Ruhr District: A holistic approach

Till Genth, Lisa Rose, Henning Jasnowski-Peters, Sebastian Westermann, Christian Melchers

Technische Hochschule Georg Agricola University, Bochum, Germany

Abstract

This study focuses on evaluating the hydraulic conductivity of the Emscher Formation as a hydraulic barrier in the Ruhr District (Germany). The aim is to build a comprehensive 3D-hydrogeological model using geological data, core samples, geophysical logs, and hydraulic tests to predict fluid and gas migration. Here, a high-resolution porosity and permeability profile from the monitoring well Pferdekamp 1, as well as quantitative mineralogical data from XRD analyses for the entire 322 m long core section, are presented. The section can be subdivided into three roughly 100 m thick compartments based on poroperm and mineralogical data. The overall permeability of the Emscher Formation ranges from K = 0.007 to 0.0007 mD using gas permeametry and porosimetry data. This research is vital in managing mine water rebound associated risks.

Keywords: Permeability, hydrogeological model, mine water rebound, Ruhr area

Introduction

Since the end of 2018, the post-mining era was initiated in the former coal mining area of the Ruhr District (Germany). Important in the post-mining phase is the controlled rise of mine water level using submersible pumps and the reduction of mine water management sites from thirteen to six. Managing mine water sustainably takes into account the evaluation of hydraulic conductivity within the Upper Cretaceous overburden formation. The Formation acts as a geological hydraulic barrier protecting ground water aquifers, especially drinking water sources, from mine water (fig. 1). During active hard coal mining, mine workings were aerated and groundwater was pumped to a level below the workings. Now, in the post-mining era, the mine water level is at various depths in separate mine water provinces. To reduce costs and make mine water management more sustainable, the mine water level needs to be raised, thus reducing pump height. To ensure the protection of drinking water sources, a buffer zone of 150 m was established between the base of freshwater formations and the mine water level. (Jasnowski-Peters & Melchers 2022). Maintaining underground water management infrastructure and integrating various water regions ensures that sections of the river Lippe remain free of mine water, which was historically used for unloading mine water. The primary goals of long term protective measures are to protect important drinking water sources for the region, minimize influence on surface water, and prevent inundation (Bezirksregierung Arnsberg 2023).

This work focuses on the scientific support of groundwater monitoring wells within the Upper Cretaceous overburden section, drilled in 2020 and commissioned by RAG AG for the project called "Tiefe Pegel". Finally, the project aims to create a comprehensive hydrogeological model based on well data from "Tiefe Pegel" integrating various analyses (petrological, sedimentological, petrophysical, borehole geophysics, and hydraulic tests). The workflow aims to retrieve petrophysical properties like permeability and porosity for the entire well profile (Bohnsack et al. 2020). The role of clay mineralogy is highlighted in correlating with hydraulic conductivity, especially swelling clays like smectites (NAGRA 2002). Detailed clay mineral analyses are crucial for inferring

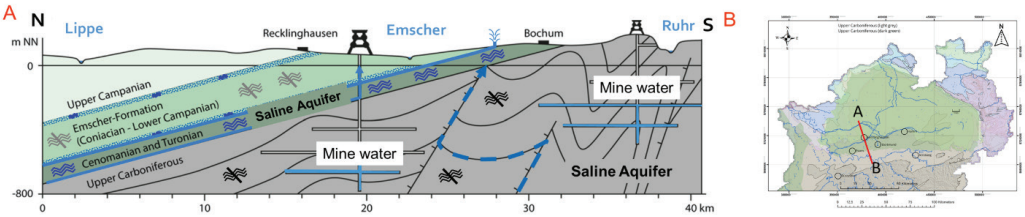

Figure 1 Geological cross section (A–B) of the Ruhr Area (modified from Hahne & Schmidt)

permeability and ensuring correct calibration of borehole geophysical data. It involves mineralogical and sedimentological analyses of core samples and cuttings, resulting in quantitative determination of swelling clay minerals using the refinement according to Rietveld (1967). Hence, a comprehensive petrological classification can be achieved, providing robust core data on porosity and permeability, which were previously lacking.

Methods

An integrated workflow that leverages laboratory data from core samples extracted from wells was constructed. Core samples of the well of Pferdekamp 1 were analysed following standard core analyses protocols including porosimetry derived and measured permeability data. The well reached a total depth of 613 m. The top of the Emscher Formation was identified with geophysical gamma ray response at 463.65 m. The final drilling depth was 780 m, including the base of the Emscher Formation at 622.00 meters. Core samples were collected every 5–10 m from a depth interval of 300 to 779.5 m.

Analyses included thin-section petrography using SEM-EDX and classical polarization microscopy using classification scheme after Folk 1951; Dunham 1962; Embry & Klovan 1971, complemented by X-ray diffraction (XRD) analysis. For XRD, clay fractions (< 2 µm) were processed as air-dried, glycolated, and heated up to > 550 °C samples (Moore & Reynolds 1997), while powder samples were measured with corundum as internal standard and quantified via Rietveld refinement analysis using the software "Profex" (Doebelin & Kleeberg 2015) and the internal Database "COD" (Vaitkus et al. 2021). Thereby, bulk XRD mineralogy was used to measure the

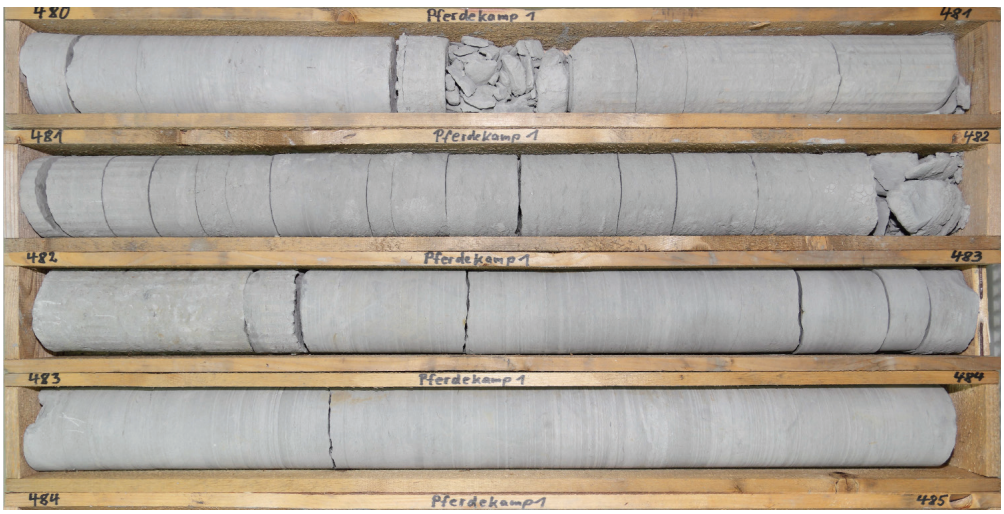

Figure 2 Core barrel from the monitoring well "Pferdekamp 1", depth 480–485 m, showing Emscher Formation marls (GD NRW 2022)

calcite content, while decarbonated samples where used to measure all other phases. The quantification was done by normalizing the calcite peaks with the decarbonated results. Grain size analyses for clay and silt fractions were conducted using a Sedigraph "Sedimat III" model by Micromeritics. Combined mineralogy and grain size analyses were used to classify the formation using the DIN 22015 protocol and define certain mineralogical compartments which were correlated with the air and porosimetry derived permeability analyses.

For porosity and permeability data, core plugs, 2.5 cm in length and diameter were drilled. Pore size distribution was determined using mercury intrusion porosimetry using an Autopore V9600 porosimeter by Micromeritics. It can measure low wettability and high surface tension, reaching mercury intrusion pressures up to 414 MPa which correspond to pore sizes as small as 3.6 nm, and up to 360 µm in diameter during extrusion to ambient pressures (Micromeritics 2017). The classical Katz and Thompson (1986) method was applied to derive permeability from porosimetry data. The Ultra-Perm 610 (Corelab), using a helium/nitrogen (He/N_2) gas flow, measured air permeability with pressures up to 17 bar (1.7 MPa), achieving precision down to 0.001 mD with air permeametry (Core Lab 2022). Adjustment according Klinkenberg (1941) was used to convert air to fluid permeability.

In-situ data from hydraulic borehole tests and geophysical logs during drilling complete these analyses. The static geological model will integrate the petrological and petrophysical characterization. To enhance model precision and reliability, laboratory results are used to calibrate geophysical logs, including resistivity and gamma-ray logs and to construct a 1 D permeability log for each monitoring well.

Results

The mineralogy is dominated by calcite, quartz and clay minerals (smectite/illite/muscovite) (fig. 3). The calcite content averages 43.7 wt.-%, making it the dominant mineralogical component in all samples. The calcite content shows a constant increase from 400 m downwards, with the highest value measured in the deepest sample at 622.57 m, reaching 84.2 wt.-%. The XRD "amorphous" residue calculated using the internal standard averages 7 wt.-%. Quartz was the second most frequently measured component in the samples. It reached concentrations ranging between 32.6 wt.-% at 482.48 m and 4.7 wt.-% at 622.57 m. Contemporary to calcite, quartz showed a reverse depth trend, with concentrations decreasing with increasing depth. The concentrations of clays including illite/muscovite and smectite also varied with depth, with the highest values being 12.6 wt.-% (at 502.50 m) and 23.4 wt.-% (at 562.50 m), respectively. Both components showed a general downward trend with increasing depth. Kaolinite/chlorite, pyrite, and rutile were present in considerably lower to trace amounts in the samples, with kaolinite/chlorite reaching a peak of 8.3 wt.-% at 402.49 m, while pyrite and rutile never exceeded 0.9 wt.-% and 0.6 wt.-%, respectively. All three components showed a downward trend with increasing depth. Specifically, pyrite was scarcely detected below 372.47 m and rutile below 362.38 m. Opal-CT was only found in the topmost samples up to a depth of 304.50 m, making up 4.4 wt.-% of the sample (fig. 3). The dataset before normalization shows a clear increase in the smectite content and a slight increase in the illite/muscovite content throughout the core. The overall proportion of smectite and illite increased, while kaolinite/chlorite and quartz showed a slight decrease. The textured samples have indicated that the mixed layers clay peak (smectite) is mostly montmorillonite with about 20–30 wt.-% of Illite. In the Pferdekamp borehole 1, DIN 22015 classifies it mainly as silty clay marlstone with an average calcite content of 41.3 wt.-%, increasing with depth. Notably, between 475 m and 482.48 m, an anti-correlation between particle sizes and mineral phases indicates a higher concentration of microquartz (< 2 µm) in the middle section.

Thin section analyses of the examined samples from the Pferdekamp 1 borehole revealed abundant nanofossils, including coccolithophorids and foraminifera of the genus Globigerinida, along with needle-like structures identified as sclerites, sponge

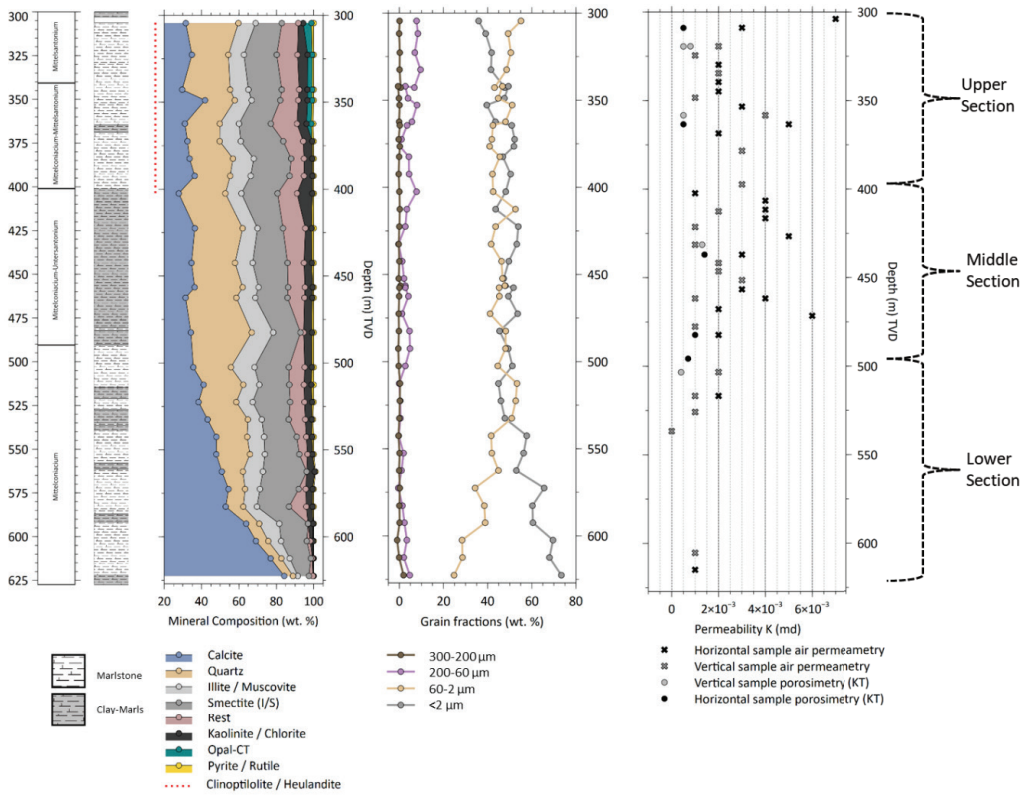

Figure 3 *Stratigraphy, macroscopic lithology, mineralogy, grain fractions and permeability (Air Permeametry and (KT) Katz-Thomson Method) of the monitoring well "Pferdekamp 1"*

spicules. Prominent quartz grains exhibited sharp structures with smooth surfaces. Pyrite crystals, framboidal aggregates and euhedral ones, were also detected within biogenic structures. A substantial portion of the thin section is composed of calcite, which displays a characteristic color spectrum under polarized light, suggesting the presence of coccolith fragments. The rock can be classified as biomikritic wackestone to packstone according to Folk and Dunham/Embry & Klovan classifications. Additionally, green minerals with a black core, identified as glauconite using scanning electron microscopy (SEM) and energy-dispersive X-ray spectroscopy (EDX) were observed. The samples also contained large areas of brownish clays where individual minerals couldn't be differentiated. Pyrite, frequently found as framboidal pyrite with sizes up to less than 1 µm, was common. The rock's visual porosity is low, with a substantial part being moldic porosity, here indicated by the blue colour of the stained thin section (fig. 4).

The Emscher Formation exhibits an average porosity of Φ = 17.5 %, with pores averaging L_c = 0.03 µm in diameter. As depth increases, there is a slight reduction in porosity. Analysis of incremental intrusion versus pore size reveals a distinct bimodality within the 0.02–0.04 µm range for two representative plugs from the Emscher Formation, indicating two main pore sizes that are evenly distributed across the samples. In terms of permeability, the Emscher Formation shows an average value of K = 0.0025 md with air-permeametry and K = 0.0007 md with the Katz-Thompson method. There is also a slight decrease in permeability towards depth (fig. 3).

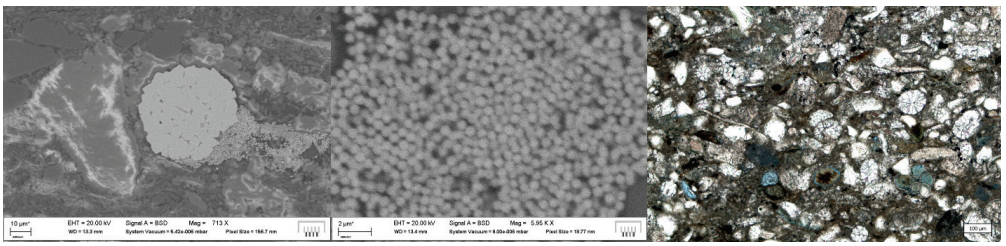

Figure 4 *Picture a and b: SEM BSD- pictures of the sample "Pferdekamp 1" (406.58 m–406.60 m) Picture c: Thin section of the sample "Pferdekamp 1" (308.7 m)*

Conclusions

The Pferdekamp 1 well section consists of marly rocks, identified mostly as biomikritic wackestone to packstone, displays intricate porosity characterized by fine to nanocrystalline elements and minimal visible porosity (fig. 4). Based on the petrological findings, the drilling of the well was divided into three distinct sections (fig. 3). This segmentation was determined by variations in mineralogical and sedimentological characteristics, which directly influence the hydraulic permeability of each section. High smectite levels in the lower section resulted in reduced permeability, while the middle section's enhanced quartz and microquartz content suggests slightly higher but still low permeability. The upper section's lower calcite and quartz content points to even lower permeability, with a consistent clay presence throughout. The topmost section, with reduced MLC (mixed layerd clay) minerals and less mature mineral phases, is likely a weak fractured aquifer (fig. 3). The ubiquitous quartz content leads to the Emscher formation's substantial porosity, which holds methane gas pockets as major threat during drilling. The overall petrological results from this drill section indicate a low permeability of the formation. In addition, the presence of mixed-layered clay (MLC) enhances the potential for sealing tectonically induced pathways.

The Emscher Marl's high porosity, at an average of Φ = 17.5 %, contrasts with its small average pore diameter of L_c = 0.03 µm, leading to very low fluid permeabilities in line with a "chalk" type petrophysical model. The bimodal distribution of pore volumes, especially in the 0.02–0.04 µm range, reflects a complex pore structure potentially trapping mercury in the process of intrusion/extrusion, consistent with the Emscher Formation's expected carbonate and siliciclastic composition.

Permeability within the Pferdekamp 1 borehole shows a decreasing trend with depth. Using Bear (1972) classification, both the measured (0.0025 mD) and calculated (0.0007 mD) permeabilities are classified a – "tight," i.e. comparable to unweathered clay or granite.

In conclusion, the formation's mineralogy and grain size-based permeability correspond with the permeability measurements based on the Katz-Thompsen and Klinkenberg adjustments. It gives a coherent picture of the formation's hydrogeological properties at the core scale.

Outlook

Upcoming efforts will involve additional core samples from the continuation of the "Tiefe Pegel" project's drilling efforts to build more groundwater monitoring wells applying this workflow. The hydrogeological model as the ultimate outcome of this project will incorporate petrological and petrophysical data in 3D to facilitate long-term predictions of fluid behavior, particularly regarding the mine water rebound.

Acknowledgements

We would like to express our gratitude to the DBM (Deutsches Bergbau-Museum Bochum) for providing XRD, SEM/EDX, and microscopy facilities. Our thanks also go to the GD NRW (Geological Survey of North Rhine-Westphalia) for insightful discussions, rock classification, and provision of sample materials. We extend our sincere appreciation to RAG AG for financial

funding and collaboration incl. data support within the project.

References

Bear, J. (1972) Dynamics of Fluids in Porous Media. New York: Dover Publications Inc.

Bezirksregierung Arnsberg (2023) Grubenwasseranstieg. Available at: https://www.bra.nrw.de/energie-bergbau/bergbaufolgen/grubenwasseranstieg.

Bohnsack, D. et al. (2020) Porosity – permeability relationship derived from Upper Jurassic carbonate rock cores to assess the regional hydraulic matrix properties of the Malm reservoir in the South German Molasse Basin, Geothermal Energy, (April). doi: 10.1186/s40517-020-00166-9.

Core Lab (2022) Ultra-Perm 610. Tulsa: Core Lab.

Doebelin, N. and Kleeberg, R. (2015) "Profex" a graphical user interface for the Rietveld refinement program "BGMN", Journal of Applied Crystallography, 48(5), pp. 1573–1580. doi: 10.1107/S1600576715014685.

Dunham, R. J. (1962) Classification of Carbonate Rocks According to Depositional Texture1, Classification of Carbonate Rocks—A Symposium. Edited by W. E. Ham. American Association of Petroleum Geologists, p. 0.

Embry, A. . and Klovan, J. E. (1971) A Late Devonian Reef Tract on Northeasterm Banks Island, Canadian Petroleum Geology, 19, pp. 730–781.

Folk, R. L. (1951) Stages of textural maturity in sedimentary rocks, Journal of Sedimentary Research. doi: 10.2110/jsr.21.127.

Jasnowski-Peters, H. and Melchers, C. (2022) Grubenwasseranstieg im ehemaligen Steinkohlenrevier des Ruhrgebiets – hydrogeochemisches Monitoring für einen nachhaltigen, öko- und ökonomisch realisierbaren Nachbergbau-Ansatz, Mining Report, 4(158), pp. 333–343.

Katz, A. J. and Thompson, A. H. (1986) Quantitative prediction of permeability in porous rock, Phys. Rev. B, 34(11), pp. 8179–8181. doi: 10.1103/PhysRevB.34.8179.

Klinkenberg, L. J. (1941) The permeability of porous media to liquids and gases., American Petroleum Institute, Drilling and Production Practice, pp. 200–213.

Micromeritics (2017) AutoPore IV Operator Manual. Norcross: Micromeritics.

Moore, D. M. and Reynolds, R. C. (1997) X-ray Diffraction and the Identification and Analysis of Clay Minerals, Clay Minerals. doi: 10.1180/claymin.1999.034.1.21.

NAGRA (2002) Technischer Bericht 02-24 Projekt Opalinuston, Synthese der geowissenschaftlichen Untersuchungsergebnisse Entsorgungsnachweis für abgebrannte Brennelemente, verglaste hochaktive sowie langlebige mittelaktive Abfälle, p. 114.

Rietveld, H. M. (1967) Line profiles of neutron powder-diffraction peaks for structure refinement, Acta Crystallographica, 22(1), pp. 151–152. doi: 10.1107/S0365110X67000234.

Vaitkus, A., Merkys, A. and Gražulis, S. (2021) Validation of the Crystallography Open Database using the Crystallographic Information Framework, Journal of Applied Crystallography, 54(2), pp. 661–672. doi: 10.1107/S1600576720016532.